Available online at www.sciencedirect.com
ScienceDirect
Mechanics of Materials 39 (2007) 787–802
MECHANICS OF MATERIALS
www.elsevier.com/locate/mechmat

Prediction of micro and nanoindentation size effect from conical or pyramidal indentation

Rashid K. Abu Al-Rub *

Department of Civil Engineering, Catholic University of America, Washington, DC 20064, USA

Received 20 August 2006; received in revised form 2 February 2007

Abstract

It is well-known by now that the hardness of the material at the micron and submicron length scales is dependent on the indent size. The objective of this work is to formulate a micromechanical-based model that can be used to predict simultaneously the indentation size effect (ISE) from both micro and nanoindentations by conical or pyramidal (Berkovich and Vickers) indenters. This model is based on the evolution of geometrically necessary dislocations (GNDs) beneath the indenter which is nonlinearly coupled to the evolution of statistically stored dislocations (SSDs) through the Taylor's hardening law. It is shown through comparisons with micro and nanoindentation experimental data that the proposed model gives much better predictions of hardness at small indentation depths as compared to the Nix–Gao model. It is concluded that when using the Taylor's hardening law a simple sum of flow stresses from SSDs and GNDs is more adequate than the simple sum of SSD and GND densities. Moreover, it is shown that the length scale responsible for the ISE is proportional to the spacing between dislocations. Thus, it is concluded that materials with smaller length scales are harder but exhibit lower ISE.

Keywords: Indentation size effect; Microindentation; Nanoindentation; Geometrically necessary dislocations; Length scale; Gradient plasticity

1. Introduction

Indentation tests have been widely used as an economical and routine method for measuring the strength and stiffness of engineering materials (Oliver and Pharr, 1992). Moreover, micro and nanoindentation techniques have become major tools for investigating the micromechanical properties of small scale volumes (e.g. thin films, nanowires, nanotubes, fibers, small particles, electronics) due to difficulty in conducting the conventional techniques and because of their fast, precise, and nondestructive merit.

However, it is well-known by now that the micro and nanoindentation hardness of metallic materials displays a strong size effect, which is commonly referred to as the indentation size effect (ISE). There are numerous indentation tests at scales on the order of a micron or a submicron have shown that the measured hardness increases significantly with decreasing the indentation size or equivalently the

* Tel.: +1 202 319 5000; fax: +1 202 319 6677.
E-mail address: rashedkamel@yahoo.com

0167-6636/$ - see front matter © 2007 Elsevier Ltd. All rights reserved.
doi:10.1016/j.mechmat.2007.02.001

indenter size (e.g. Stelmashenko et al., 1993; De Guzman et al., 1993; Ma and Clarke, 1995; Poole et al., 1996; McElhaney et al., 1998; Lim and Chaudhri, 1999; Elmustafa and Stone, 2002; Gerberich et al., 2002; Swadener et al., 2002; Huber et al., 2002; Abu Al-Rub and Voyiadjis, 2004a). This has been attributed to the evolution of the so-called geometrically necessary dislocations (GNDs) beneath the indenter, which gives rise to strain gradients (Ashby, 1970; Arsenlis and Parks, 1999). The classical continuum plasticity theory predicts a constant hardness when using a geometrically self-similar indenter on a homogenous material and cannot predict the ISE since it does not possess an intrinsic material length scale. On the other hand, it is still not possible to perform quantum and atomistic simulations on realistic time scale and structures. There are, however, many dislocations at the micron scale (around 30 per micron in each direction for a dislocation density of $10^{15}\mathrm{m}^{-2}$) such that their collective behavior on plastic work hardening of materials should be characterized by a continuum (but not classical) plasticity model. Moreover, there are several other size effects besides the ISE that are attributed to the evolution of GNDs and could not be explained by the classical continuum plasticity theory. For example, experimental work has revealed that a substantial increase in the macroscopic flow stress can be achieved by decreasing the particle size of particle-reinforced composites while keeping the volume fraction constant (e.g. Lloyd, 1994; Nan and Clarke, 1996; Kiser et al., 1996), by decreasing the diameter of thin wires in microtorsion test (Fleck et al., 1994), and with decreasing the thickness of thin films in microbending test (Stolken and Evans, 1998; Shrotriya et al., 2003; Haque and Saif, 2003).

The strain gradient plasticity theories, which are founded on the GND's concept, have given reasonable agreement with the ISE and other size effects since it incorporates an intrinsic material length scale in the constitutive equations [see Abu Al-Rub and Voyiadjis (2006) for an extensive review of these theories]. However, the full utility of the strain gradient plasticity theories hinges on one's ability to determine the constitutive length parameter that scales the gradient effect. The study of Begley and Hutchinson (1998), Yuan and Chen (2001), Abu Al-Rub and Voyiadjis (2004a,b) indicated that indentation experiments may be the most effective test for measuring the length scale parameter. However, the study of Abu Al-Rub and Voyiadjis (2004a) and Voyiadjis and Abu Al-Rub (2005) have indicated that this length scale parameter is not a constant for a given material but it depends on the spacing between dislocations, which is deformation dependent.

By considering the GNDs generated by a conical indenter, Nix and Gao (1998) developed an ISE model that suggests a linear dependence of the square of the microhardness to the inverse of the indentation depth. Swadener et al. (2002) utilized the basic precepts given by Nix and Gao (1998) for a conical indenter and developed an ISE model for spherical indenters which suggests a linear dependence of the square of the microhardness to the inverse of the diameter of the indenter. However, recent micro and nanoindentation results show that the predictions of the Nix–Gao and Swadener et al. models deviate significantly from the experimental results at small indentation depths (i.e. nanoindentation) in the case of Berkovich and Vickers indenters (e.g. Lim and Chaudhri, 1999; Saha et al., 2001; Elmustafa and Stone, 2002; Feng and Nix, 2004; Abu Al-Rub and Voyiadjis, 2004a; Manika and Maniks, 2006) and at small diameters for the case of spherical indenters (Swadener et al., 2002; Abu Al-Rub and Voyiadjis, 2004a). Moreover, Elmustafa and Stone (2002) observed that when the Nix–Gao model is used to fit the experimental results of micro and nanohardness, the data at deep indents (microhardness) exhibits a straight-line behavior whereas for shallow indents (nanohardness) the slope of the line severely changes, decreasing by a factor of 10, resulting in a bilinear behavior and, therefore, two different values for the material length scale are used to fit the micro and nanoindentation data. Recently, Huang et al. (2006) modified the Nix–Gao model by reducing the density of GNDs at small indentation depths where two values for the material length scale are also used to fit the micro and nanoindentation data. Therefore, Nix–Gao model can fit well either the hardness data from microindentation or nanoindentation tests, but not both simultaneously. Yuan and Chen (2001), Qiu et al. (2001), and Swadener et al. (2002) have modified the Nix–Gao model by incorporating the effect of intrinsic lattice resistance or friction stress. However, it is shown by Huang et al. (2006) that the inclusion of the friction stress gives better predictions than the Nix–Gao model but still is not satisfactory to give well predictions of the nanoindentation results. Moreover, Xue et al. (2002), and Qu et al. (2004) have attributed

the deviation of the Nix–Gao model from nanoindentation hardness data to the rounded shape of conical or pyramidal indenter real tips and, therefore, Alkorta et al. (2006) refined the Nix–Gao model by taking into account the tip roundness. However, it is shown in Huang et al. (2006) that the indenter tip radius effect alone cannot explain the nanoindentation size effect. Zhao et al. (2003) further refined the Nix–Gao model by considering the nonuniform distribution of GND density underneath the indenter. Feng and Nix (2004) and Durst et al. (2006) reformulated the Nix–Gao model by assuming that the GNDs are stored within the plastically deformed zone of size greater than the contact radius of indentation, which is somewhat similar to the modification proposed by Huang et al. (2006). Moreover, it is shown in this paper that this modification does not affect the qualitative behavior of the Nix–Gao model, but significantly affects the calibrated value of the material length scale. Therefore, all of the aforementioned remedies to the Nix–Gao ISE model gave a marginal improvement to the predictions of nanoindentation hardness data such that none of the aforementioned modified models could be used to predict both micro and nanoindentation results satisfactorily. Abu Al-Rub and Voyiadjis (2004a,b) suggested that the most likely impediment in the Nix–Gao model is the assumption that the densities of SSDs and GNDs are coupled in a linear sense through the Taylor's hardening law and, therefore, a nonlinear coupling should be enhanced. This suggestion is the main focus of this paper.

Despite the fact that the ISE has been reported by many well-reputed experimental groups, there are still points of controversy in predicting and understanding the mechanism of this type of size effect. This study shed some insight on interpretation of the ISE encountered in micro and nanohardness from conical or pyramidal indenters. An ISE analytical model that can predict equivalently well the micro and nanoindentation hardness data from conical/pyramidal indentation is formulated using a micromechanical model that assesses a nonlinear coupling between the densities of SSDs and GNDs. The employed micromechanical model, which is based on the Taylor's hardening law, is used to link the strain gradient effect at the microscopic scale with the stress-strain behavior of an equivalent continuum with homogenized plastic deformation at the mesoscopic level. This constitutive framework yields an expression for the deformation-gradient-related intrinsic length scale parameter ℓ in terms of measurable microstructural physical parameters. Moreover, the proposed ISE model is successful in predicting the hardness results from both micro and nanoindentation tests and can be used to identify the magnitudes of the material length scale parameter.

2. Physical interpretation of the material length scale

Generally, it is assumed that the total dislocation density represents the total coupling between two types of dislocations which play a significant role in the hardening mechanism. Material deformation in metals enhances the dislocation formation, the dislocation motion, and the dislocation storage. The dislocation storage causes material hardening. The stored dislocations generated by trapping each other in a random way are referred to as statistically stored dislocations (SSDs), while the stored dislocations that relieve the plastic deformation incompatibilities within the polycrystal caused by nonuniform dislocation slip are called geometrically necessary dislocations (GNDs). Their presence causes additional storage of defects and increases the deformation resistance by acting as obstacles to the SSDs (Arsenlis and Parks, 1999). Therefore, as far as the experimental findings up to day, one cannot assume that GNDs are similar to SSDs since both are different in nature. The SSDs are believed to be dependent on the effective plastic strain, while the density of GNDs is directly proportional to the gradient of the effective plastic strain (Ashby, 1970). Moreover, non-vanishing net Burgers vector from the excess of dislocations of one sign in any region bounded by a closed curve implies the existence of GNDs (Nye, 1953; Arsenlis and Parks, 1999). Therefore, an easy way to distinguish if the material possesses GNDs is by computing the net Burgers vector. SSDs conserve the net Burgers vector of the volume in which they occur, whereas the divergence of dislocation density flux leads to a net change in the Burgers vector of the volume. For more details about different interpretations of the physical nature and properties of SSDs and GNDs the reader is referred to the complete issue in Scripta Materialia (Needleman and Gil Sevillano, 2003).

The densities of SSDs and GNDs can be combined in various ways for which there is little guidance from dislocation mechanics. Mughrabi (2001) concluded that the simple superposition of the density of GNDs on the density of SSDs is *not well*

founded and they are unambiguously related. Abu Al-Rub and Voyiadjis (2004a,b) and Voyiadjis and Abu Al-Rub (2005) presented different phenomenological forms to enhance the nonlinear coupling between SSDs and GNDs. One possible coupling can be assessed by writing the overall flow stress, σ, as follows:

$$\sigma = \sigma_y + \left[\sigma_S^\beta + \sigma_G^\beta\right]^{1/\beta} \tag{1}$$

where σ_y is the initial yield stress, and β is considered as a material constant, termed here the *interaction coefficient*, and used to assess the sensitivity of predictions to the way in which the coupling between the SSDs and GNDs is enhanced during the plastic deformation process. Thus, different values of β implies changes in the strain history. The general form in Eq. (1) ensures that $\sigma \to \sigma_y + \sigma_S$ whenever $\sigma_S \gg \sigma_G$ (i.e. classical plasticity) and that $\sigma \to \sigma_y + \sigma_G$ whenever $\sigma_S \ll \sigma_G$. The stresses σ_S and σ_G are associated respectively with the densities of SSDs and GNDs through the Taylor's hardening law as follows:

$$\sigma_S = m\alpha Gb\sqrt{\rho_S}, \quad \sigma_G = m\alpha Gb\sqrt{\rho_G} \tag{2}$$

where m is the Taylor factor, which acts as an isotropic interpretation of the crystalline anisotropy at the continuum level; $m = \sqrt{3}$ for an isotropic solid and $m = 3.08$ for FCC polycrystalline metals (Taylor, 1938), G is the shear modulus, b is the magnitude of Burgers vector, and α is a statistical coefficient between 0.1 and 0.5. The empirical constant α accounts for the deviation from regular spatial arrangements of the SSD and GND populations. For impenetrable forest dislocations, Kocks (1966) assumed $\alpha = 0.85$ for SSDs and Busso et al. (2000) assumed $\alpha = 2.15$ for GNDs. For simplicity, in the present work it is assumed that α is the same for both SSDs and GNDs.

It is noteworthy that Eq. (2) implies that SSDs and GNDs are similar in nature concerning their properties, but the process of their nucleation, motion, storage, and annihilation are different. The SSDs density evolves through Burgers vector-conserving reactions based on dislocation mechanics while the GNDs density evolves due to the divergence of dislocation fluxes associated with the inhomogeneous nature of plasticity in crystals (Arsenlis et al., 2004; Abu Al-Rub and Voyiadjis, 2006). It is beleived that SSDs are generated first and then some of these SSDs become geometrical (mainly at grain boundaries and interfaces) and others are trapped due to interaction with obstacles or other dislocations (statistical or geometrical). Therefore, both SSDs and GNDs increase/decrease in density as deformation progresses and both contribute to material hardening. Moreover, the evolution of GNDs does not necessarily increase the total dislocation density. It may also decrease the total density. Whether dislocation density is accumulated or lost due to the flux divergence depends on the participation of the relative densities to the plastic deformation across the volume and on the sign of their divergence. For example, if positive edge dislocations are the only ones within a volume and the plastic strain field is such that more edge dislocations leave the volume than enter the volume, the total dislocation density in the volume will decrease as a result of the inhomogeneous plastic deformation (Arsenlis et al., 2004). However, fundamental research at the discrete dislocation level with using the principles in dislocation mechanics is needed for the proper physical interpretation of the evolution and interaction between SSDs and GNDs.

Strain gradients play an essential role in the prediction of size effects in the deformation behavior of metals at the mesoscale scale. The classical plasticity, which inherently includes no material length scale, cannot predict size effects. Strain gradient plasticity theories extend the classical plasticity models by including an intrinsic material length scale and are therefore appropriate for problems involving small dimensions. Motivated by the Taylor law in Eq. (1) at the micromechanical level, one can therefore assume the following power-law of the corresponding gradient-dependent flow stress at the mesoscale (Abu Al-Rub and Voyiadjis, 2004a; Voyiadjis and Abu Al-Rub, 2005):

$$\sigma = \sigma_y + \sigma_0\left(\widehat{\varepsilon}^p\right)^{1/n} \quad \text{with} \quad \widehat{\varepsilon}^p = \left[(\varepsilon^p)^\gamma + (\ell\eta)^\gamma\right]^{1/\gamma} \tag{3}$$

where $\gamma = \beta/2$, σ_0 is a measure of the yield stress in uniaxial tension, ℓ is the material length scale, $n \geqslant 1$ is the hardening exponent, $\widehat{\varepsilon}^p$ and ε^p are the nonlocal and local effective plastic strains, respectively, η is an effective measure of the gradient of plastic strain which is related to the GND density.

During plastic deformation, the density of SSDs increases due to a wide range of processes that leads to production of new dislocations. Those new generated dislocations travel on a background of GNDs which act as obstacles to the SSDs. If L_S is the average distance traveled by a newly generated disloca-

tion, then the rate of accumulation of strain due to SSDs scales with $\dot{\varepsilon}^p \propto L_S b \dot{\rho}_S$ (Orowan, 1948) such that for proportional loading and monotonically increasing plasticity, one can express ε^p in terms of ρ_S (Abu Al-Rub and Voyiadjis, 2004a,b):

$$\varepsilon^p = \frac{1}{m} b L_S \rho_S \tag{4}$$

Ashby (1970), Arsenlis and Parks (1999), and Gao et al. (1999) showed that gradients in the plastic strain field are accommodated by the GND density, ρ_G, such that the effective strain gradient η that appears in Eq. $(3)_2$ can be defined as follows:

$$\eta = \frac{\rho_G b}{\bar{r}} \tag{5}$$

It is shown that this expression allows η to be interpreted as the deformation curvature in bending and the twist per unit length in torsion (e.g. Fleck et al., 1999; Gao et al., 1999; Voyiadjis and Abu Al-Rub, 2005; Abu Al-Rub and Voyiadjis, 2006). The constant $\bar{r} \approx 2$ is the Nye's factor introduced by Arsenlis and Parks (1999) to reflect the scalar measure of GND density resultant from mesoscopic plastic strain gradients.

Now substituting Eqs. (4) and (5) into Eq. (3) and comparing the result with Eq. (1) after substituting Eq. (2) yields the following expression for the intrinsic material length scale ℓ in term of the mean free path of dislocations L_S:

$$\ell = \hbar L_S \quad \text{with } \hbar = \bar{r}/m \tag{6}$$

which also gives σ_0 as

$$\sigma_0 = G\sqrt{\alpha^2 m^3 b / L_S} \tag{7}$$

The microstructural length scale parameter, ℓ, and the phenomenological measure of the yield stress in uniaxial tension, σ_0, are now related to measurable physical parameters. The form and magnitude of ℓ depends on the dominant mechanism of plastic flow at the scale under consideration. It appears from Eq. $(6)_1$ that the size effect and its implications on the flow stress and work-hardening is fundamentally controlled by the dislocation glide, which is deformation dependent. If one assumes $m \approx 2$ and $\bar{r} \approx 2$ then $\ell \approx L_S$, which can be experimentally measured. Therefore, L_S is a crucial physical measure that controls the evolution of the length scale in gradient plasticity theory for metals such that the key feature of plastic deformation is the reduction of the free path, cell size, or spacing between dislocations with strain.

It is noteworthy that Eq. (7) is valid when setting the hardening exponent $n = 2$ which is not unreasonable for some materials (Nix and Gao, 1998), particularly for some annealed crystalline solids. However, the author believes that the origin of this condition stems out from the assumption that the Taylor's flow stress is directly proportional to the square root of the dislocations density ρ (i.e. $\sigma \propto \sqrt{b^2\rho}$), which can be rewritten as $\rho^{1/n}$ with $n = 2$. More generally, one can assume that $\sigma \propto (b^2\rho)^{1/n}$ with $n \geqslant 1$.

Moreover, by substituting L_S from Eq. $(6)_1$ into Eq. (7), one obtains a relation for ℓ as a function of the shear modulus, yield stress, and other microstructural parameters, such that:

$$\ell = m^2 \alpha^2 \bar{r} (G/\sigma_0)^2 b \tag{8}$$

If one sets $m = 3.08$, $\alpha = 0.3$, $b = 0.225$ nm, $G/\sigma_0 = 100$, then $\ell = 3.8$ μm which is a physically sound value in the range of micrometers as reported by many authors in the material community (e.g. Begley and Hutchinson, 1998; Nix and Gao, 1998; Stolken and Evans, 1998; Yuan and Chen, 2001; Zhao et al., 2003; Abu Al-Rub and Voyiadjis, 2004a,b).

3. Model for the indentation size effect

Conical or pyramidal indents whose sizes exceed tens of microns generally produce size-independent hardness values in most metals and can be considered as large indents. Smaller indents in the range from submicron to about 10 μm in single crystals or fine-grained polycrystals often display a significant size effect. For example, the hardness inferred from pyramidal indents on the order of 1 μm in width can be two or three times the hardness obtained from an indent that is 10 μm across. A clear understanding of the ISE and its connection with the material strength is especially important in modern applications involving thin films and multilayers since micro and nanoindentation are frequently the only means of measuring their mechanical properties.

In this section a simple analytical model that can be used to predict equivalently both micro and nanohardness when using conical or pyramidal (Berkovich and Vickers) indenters is proposed based on the concept of GNDs.

Tabor (1951) showed in his experiments that the elasto-plastic material response in tensile testing could be correlated to the response in conical/pyramidal (Berkovich and Vickers) indentation. The

fundamental parameters for indentation tests by conical/pyramidal indenter are (see Fig. 1): the force applied to the indenter, P, the residual contact radius of indentation, a_p, the hardness, $H = P/\pi a_p^2$, the permanent indentation depth, h_p, the total indentation depth, h, the plastic zone radius, c_p, and the indenter geometry; i.e. the angle between the surface of the conical indenter and the plane of the surface θ. This angle is related to h_p and a_p by $\tan\theta = h_p/a_p$ (see Fig. 1). The unloading process in the indentation experiment is essential for the proper specification of these geometric parameters. Thus, the residual values h_p and a_p should be used as measurable data in the hardness H calculations.

Consider now the indentation by a rigid cone, as shown schematically in Fig. 1. One can assume that the density of GNDs is integrated by the geometry of the indenter and the indentation is accommodated by circular loops of GNDs with Burgers vectors normal to the plane of the surface. One can use the simple model of GNDs developed by Stelmashenko et al. (1993), De Guzman et al. (1993), Nix and Gao (1998), and Abu Al-Rub and Voyiadjis (2004b) to determine the density of GNDs evolved under a conical/pyramidal indenter. As the indenter is forced into the surface of a single crystal, GNDs are required to account for the permanent shape change at the surface. Of course SSDs, not shown in Fig. 1, would also be created and they would contribute to the deformation resistance.

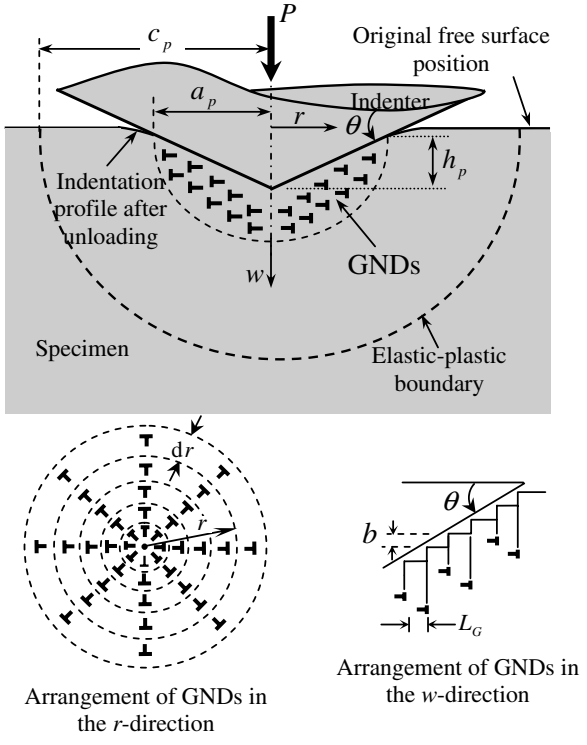

Fig. 1. Axisymmetric rigid conical indenter. Geometrically necessary dislocations created during the indentation process. The dislocation structure is idealized as circular dislocation loops.

The indentation profile in the unloaded configuration when using conical/pyramidal indenters can be described by (see Fig. 1):

$$w(r) = h_p - r(\tan\theta) \quad \text{for } 0 \leqslant r \leqslant a_p \tag{9}$$

If one assumes that the individual dislocation loops of GNDs as being spaced equally along the surface of the indentation, as shown in Fig. 1, then it is easy to show that:

$$\left|\frac{dw}{dr}\right| = \frac{b}{L_G} = \tan\theta = \frac{h_p}{a_p} \Rightarrow L_G = \frac{ba_p}{h_p} \tag{10}$$

where L_G is the mean spacing between individual slip steps on the indentation surface corresponding to the GND loops. If λ is the total length of the injected loops, then between r and $r + dr$ one can write:

$$d\lambda = 2\pi r\frac{dr}{L_G} = 2\pi r\frac{h_p}{ba_p}\,dr \tag{11}$$

Integrating from 0 to a_p gives the total length of GND loops as:

$$\lambda = \int_0^{a_p} 2\pi r\frac{h_p}{ba_p}\,dr = \frac{\pi a_p h_p}{b} \tag{12}$$

It is assumed that the dislocation evolution during indentation is primarily governed by a large hemispherical volume V that scales with the contact radius a_p around the indentation profile (see Fig. 1). However, the GNDs reside inside a plasticity zone which can be viewed as extending to a radius c_p to the outermost dislocation emanated from the indent core. Therefore, the size of the plastic zone, c_p, underneath the indenter is larger than the contact radius, a_p, as suggested by Feng and Nix (2004) and Durst et al. (2006) such that $c_p = fa_p$ where $f > 1$, which will be defined later in this section, can be interpreted as the ratio of the plastic zone radius to contact radius. One can then assume that all the injected GND loops remain within a hemispherical volume V of radius c_p, such that:

$$V = \frac{2}{3}\pi c_p^3 = \frac{2}{3}\pi f^3 a_p^3 \tag{13}$$

Therefore, the density of GNDs becomes

$$\rho_G = \frac{\lambda}{V} = \frac{3}{2f^3 b h_p}\tan^2\theta \tag{14}$$

The GND density is reduced by using a bigger storage volume at small indentation depth. In reality the GND density cannot be very large because of the strong repulsive forces between GNDs which push dislocations to spread beyond the hemisphere at small indentation depth (Swadener et al., 2002).

Tabor (1951) specified the mapping from the $H-h$ curve to $\sigma-\varepsilon^p$ curve such that one can express the micro/nanohardness as:

$$H = \kappa\sigma = H_y + \kappa m\alpha b G\left[(\rho_S)^{\beta/2} + (\rho_G)^{\beta/2}\right]^{1/\beta} \tag{15}$$

where Eqs. (1) and (2) are used in obtaining the above expression. $H_y = \kappa\sigma_y$ is the hardness due to the initial yield stress σ_y. The parameter κ is the Tabor's factor from 2.8 to 3.07. The Tabor's relation (i.e. $H = \kappa\sigma$) has been extensively verified and used by many authors in the literature and, therefore, one may indeed take it as a starting point.

Based on the assumption of a self-similar deformation field (Hill et al., 1989; Biwa and Storakers, 1995), it was shown that the displacement is proportional to the indentation depth h_p. Based on this observation, Xue et al. (2002) showed from numerical experiments that the strain field should depend only on the normalized indentation depth, h_p/a_p, such that one may assume that the effective plastic strain ε^p is defined by:

$$\varepsilon^p = c(h_p/a_p) = c\tan\theta \tag{16}$$

where c is a material constant from 0.2 to 0.4. It can be noted from Eq. (16) that the plastic strain is independent of the indentation depth.

Considering Eqs. (4), (6) and (16) yields the following expression for the density of SSDs:

$$\rho_S = \frac{c\bar{r}\tan\theta}{\ell b} \tag{17}$$

The macrohardness H_0 is defined as the hardness that would arise from SSDs alone in the absence of GNDs, that is, the hardness that corresponds to the saturation value where the hardness H does not change as the indentation depth h_p increases, or that predicted by conventional plasticity theory, such that one can write from Eq. (15):

$$H_0 = H_y + \kappa m\alpha b G\sqrt{\rho_S} \tag{18}$$

Substituting Eqs. (14) and (17) into Eq. (15) with the use of Eq. (18), one can obtain the following ISE model:

$$\left(\frac{H-H_y}{H_0-H_y}\right)^{\beta} = 1 + \left(\frac{h^*}{h_p}\right)^{\beta/2} \tag{19}$$

where h^* and H_0 are, respectively, given by:

$$h^* = \zeta\ell \quad \text{with } \zeta = \frac{3}{2f^3 c\bar{r}}\tan\theta \tag{20}$$

$$H_0 = H_y + \kappa\sigma_0 c^{1/n}(\tan\theta)^{1/n} \tag{21}$$

The parameter h^* is a material parameter that characterizes the depth dependence of the hardness and depends on the material length scale, ℓ, indenter geometry, θ, and the plastic flow through f, c, and $\bar{r}$. Thus, h^* is a crucial parameter that characterizes the ISE and its accurate experimental measure gives a reasonable value for ℓ.

By assuming that both SSDs and GNDs are coupled in a linear sense, i.e. $\beta = 2$ as will be shown later in Section 5, neglecting the friction hardness (i.e. $H_y = 0$), and assuming all the GNDs are stored in a plastic zone of radius equal to the contact radius a_p (i.e. $f = 1$), one retains from Eq. (19) the commonly-used ISE model of Nix and Gao (1998):

$$\left(\frac{H}{H_0}\right)^2 = 1 + \left(\frac{h^*}{h_p}\right) \tag{22}$$

Moreover, Nix and Gao (1998) suggested that h^* and H_0 are dependent and related through $h^* = (81/2)b\alpha^2\tan^2\theta(G/H_0)^2$. Their relation, thus, gives a similar argument to that of Eq. (20) which suggests that h^* is dependent on the shape of the indenter as well as on the material property.

The hardness H from Eq. (19) is dependent on the value of the interaction coefficient β, which is considered here as a fitting factor. Therefore, when fitting the experimental data to the proposed ISE model, one of the key issues is the suitable choice for a value of β. As seen in Eq. (1), this parameter has a physical meaning, where it reflects the degree of interaction between the SSD density, ρ_S, and the GND density, ρ_G. In Fig. 2 group of size-dependent hardness curves are plotted with various β values ranging from 0.7 to 2. It is evident that while the β effect is significant especially at lower β values, all the curves show a strong ISE. The value of $\beta = 2$ corresponds to the Nix–Gao model. It can be noticed that the hardness is progressively increasing as the indentation depth decreases, but with a lower rate for $\beta < 2$ as compared to the Nix–Gao

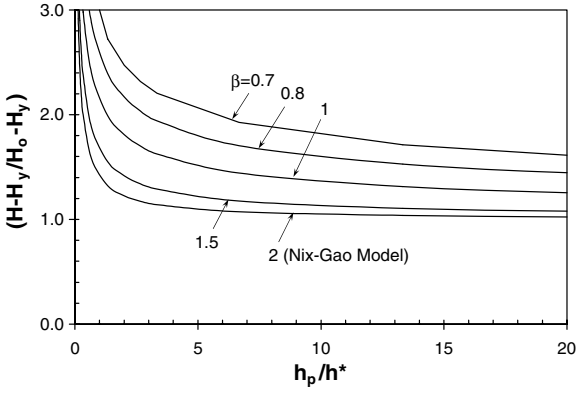

Fig. 2. Normalized hardness versus normalized indentation depth with different values of β.

model. Furthermore, Abu Al-Rub and Voyiadjis (2004a) have pointed out that in general β should be less than or equal to 1, so that a higher interaction is obtained. Therefore, it is argued here that $\beta < 2$ is successful in reproducing the deviation from the Nix–Gao relationship occurring at very low indentation depths as is shown in the subsequent sections.

One can easily show that the ISE in conical/pyramidal indentation can be interpreted by a decrease in hardness with an increase in the residual contact radius a_p simply by substituting for h_p in Eq. (19) the relation $h_p = a_p \tan\theta$, such that:

$$\left(\frac{H - H_y}{H_0 - H_y}\right)^{\beta} = 1 + \left(\frac{a^*}{a_p}\right)^{\beta/2} \tag{23}$$

where a^* is given in terms of ℓ by

$$a^* = \varsigma \ell \quad \text{with } \varsigma = \frac{3}{2f^3 c\bar{r}} \tag{24}$$

The expression in Eq. (23) shows that H increases with decreasing the contact radius a_p (i.e. GNDs decreases with increasing a_p, $\rho_G = 3\tan\theta/2b_G a_p$). Furthermore, Eq. (24) shows that ℓ is independent of the indenter geometry (i.e. θ) when the ISE is interpreted by Eq. (23).

The size of the plastic zone, c_p, in Eq. (13) can be calculated using the following well-established relation (e.g. Johnson, 1970; Kramer et al., 1999; Chiu and Ngan, 2002):

$$c_p = \sqrt{\frac{3P}{2\pi\sigma_y}} \tag{25}$$

Substituting in the above expression $H = P/\pi a_p^2$, which is size dependent, with $H_y = \kappa\sigma_y$ and $c_p = f a_p$ yields the ratio of plastic zone size to contact radius as $f = \sqrt{\frac{3}{2}\kappa H/H_y}$. However, $P/\pi c_p^2$ is observed experimentally to be roughly constant with respect to the indent size (Chiu and Ngan, 2002), and this means that H is roughly constant at $r = c_p$. This suggests that the indentation hardness near the elastic–plastic boundary is already approximately self-similar and is not affected by size dependent events at the indent core. It seems, therefore, that at $r = c_p$ one can set $H = H_y$, which gives the factor $f = \sqrt{\frac{3}{2}\kappa}$ such that f is constant. Substituting $\kappa = 3$ gives $f = 2.12$, which is in the range of the experimental values reported by Kramer et al. (1999), Feng and Nix (2004), and Durst et al. (2006). Moreover, Feng and Nix (2004) suggested a dependence of f on the indentation depth based on phenomenological aspects and not physical ones. However, the significance of this proposition will be evaluated in a future work.

It is noteworthy that the present interpretation of the ISE is based on the evolution of the GNDs, while from time to time in the literature several important factors in experiments (e.g. interfacial friction, indenter pile-up or sink-in, loading rate, oxidation layer, etc.) have been thought to be responsible for the ISE. However, careful experimental studies by Xue et al. (2002) have excluded these factors from being completely responsible for the ISE.

4. Comparing with experimental results

All the experiments used here in validating the proposed model, Eq. (19), are conducted at room temperature and using a Berkovich or Vickers pyramidal indenters for which the nominal or projected contact area varies as:

$$A_c = 24.5h^2 = \pi a^2 \tag{26}$$

Using this relation together with $\tan\theta = h_p/a_p$ yields:

$$\tan\theta = \sqrt{\frac{\pi}{24.5}} = 0.358 \tag{27}$$

Lim and Chaudhri (1999), Swadener et al. (2002), Elmustafa and Stone (2002), and Feng and Nix (2004) have conducted experimental investigations on OFC, iridium, alpha-brass, and MgO, respectively, using micro and nanoindentation in order to study the ISE when using pyramidal indenters. The hardness experimental data obtained from

nano and microindentations using, respectively, Berkovich and Vickers indenters are plotted in Figs. 4a–f as the hardness H versus the indentation depth h_p.

The characteristic form for the ISE presented by either Eq. (19) or Eq. (23) gives a straight line when the hardness data are plotted as $(H - H_y/H_0 - H_y)^\beta$ versus $h_p^{-\beta/2}$ or $a_p^{-\beta/2}$, the intercept of which is one and the slope is $h^{*\beta/2}$ or $a^{*\beta/2}$, respectively. Three parameters are identified by obtaining this fit, which are β, h^* (or a^*), and H_y. For example, this fitting procedure is presented in Fig. 3a using Eq. (19) by plotting the annealed iridium hardness data of Swadener et al. (2002). The interaction parameter $\beta = 0.8$ is chosen such that the best linear fit is obtained for both micro and nanoindentation hardness data, which yields $h^* = 0.3$ μm. The macroscopic hardness $H_0 = 2.4$ GPa is obtained when the hardness curve reaches plateau at large indentation depths [see Fig. 4a]. The yield hardness $H_y = 0.305$ GPa, which is the work hardening component representing the increase in hardness from the onset of yielding, is calculated using $H_y = \kappa\sigma_y$ with $\kappa = 2.8$ and $\sigma_y = 0.109$ GPa, where the value of σ_y is obtained by Swadener et al. (2002) using a uniaxial tensile test. It can be seen from Fig. 3a that the proposed model fits very well both the micro and nanoindentation hardness data.

Nix and Gao (1998) proposed plotting their model in Eq. (22) as $(H/H_0)^2$ versus $1/h_p$, which should result in a straight line with slope h^*. Fig. 3b fits well only the microindentation hardness data of annealed iridium with $H_0 = 2.5$ GPa and $h^* = 2.15$ μm, but significantly overestimates the nanoindentation hardness data.

The fitting procedures as described above for both the present model and the Nix–Gao model are repeated for the remaining hardness data of Lim and Chaudhri (1999), Elmustafa and Stone (2002), and Feng and Nix (2004). In Figs. 4a–f comparisons between the predictions of the present model, Eq. (19), and that of the Nix–Gao model, Eq. (22), are shown. The values of β, H_y, H_0, and h^* used to fit the experimental results are shown in the figures.

Table 1 shows a summary of the values for β, H_y, H_0, and h^* used to fit the experimental results by the present ISE model in Eq. (19). The dimensionless parameter $\zeta = 0.141$, which is used to estimate the material length scale parameter ℓ in Table 1, is calculated from Eq. $(20)_2$ by assuming that $c = 0.2$ [corresponds to 7% effective plastic strain as reported by Johnson (1970) when using pyramidal indentation], the Nye factor $\bar{r} = 2$ (Arsenlis and Parks, 1999), the plastic zone ratio $f = 2.12$, and $\tan\theta = 0.358$. The calculation of ℓ, therefore, strongly depends on the material parameters c, $\bar{r}$, and f.

It can be seen from Fig. 4a–f that the present model predictions agree well with both the micro and nanohardness data, while the predictions of the Nix–Gao model diverge significantly from the nanohardness results for $h_p < 1$ μm except for MgO where Nix–Gao model overpredicts the nanohardness at $h_p < 0.2$ μm. It can also be noted from Table 1 and Fig. 4a–f that ideally the macroscopic hardness H_0 from the Nix–Gao model and $H_0 + H_y$ from the present model should be the same since H_0 is independent of GNDs. However, in fitting the present model to the experimental data,

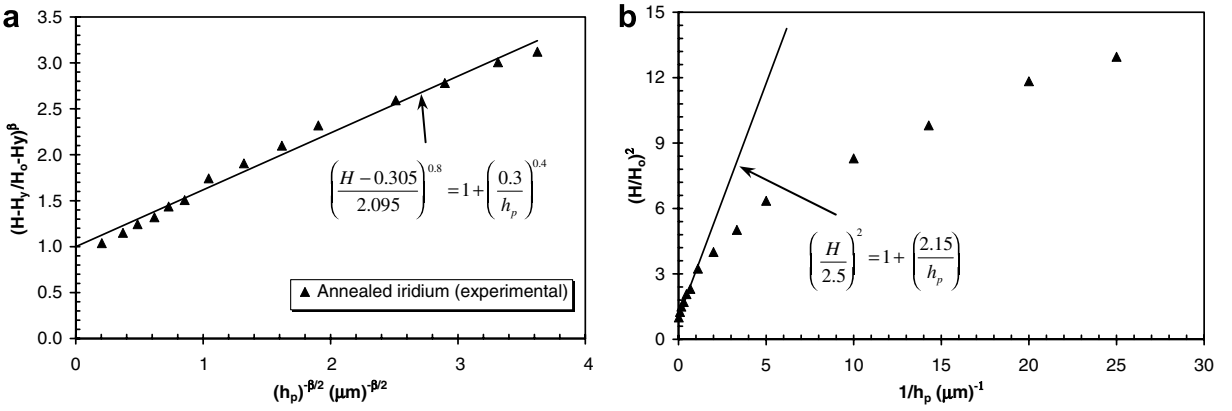

Fig. 3. The fitting procedures for both (a) the present model, Eq. (19), and (b) the Nix and Gao (1998) model, Eq. (22). The solid line is a linear curve fit of the experimental hardness results for annealed iridium by Swadener et al. (2002).

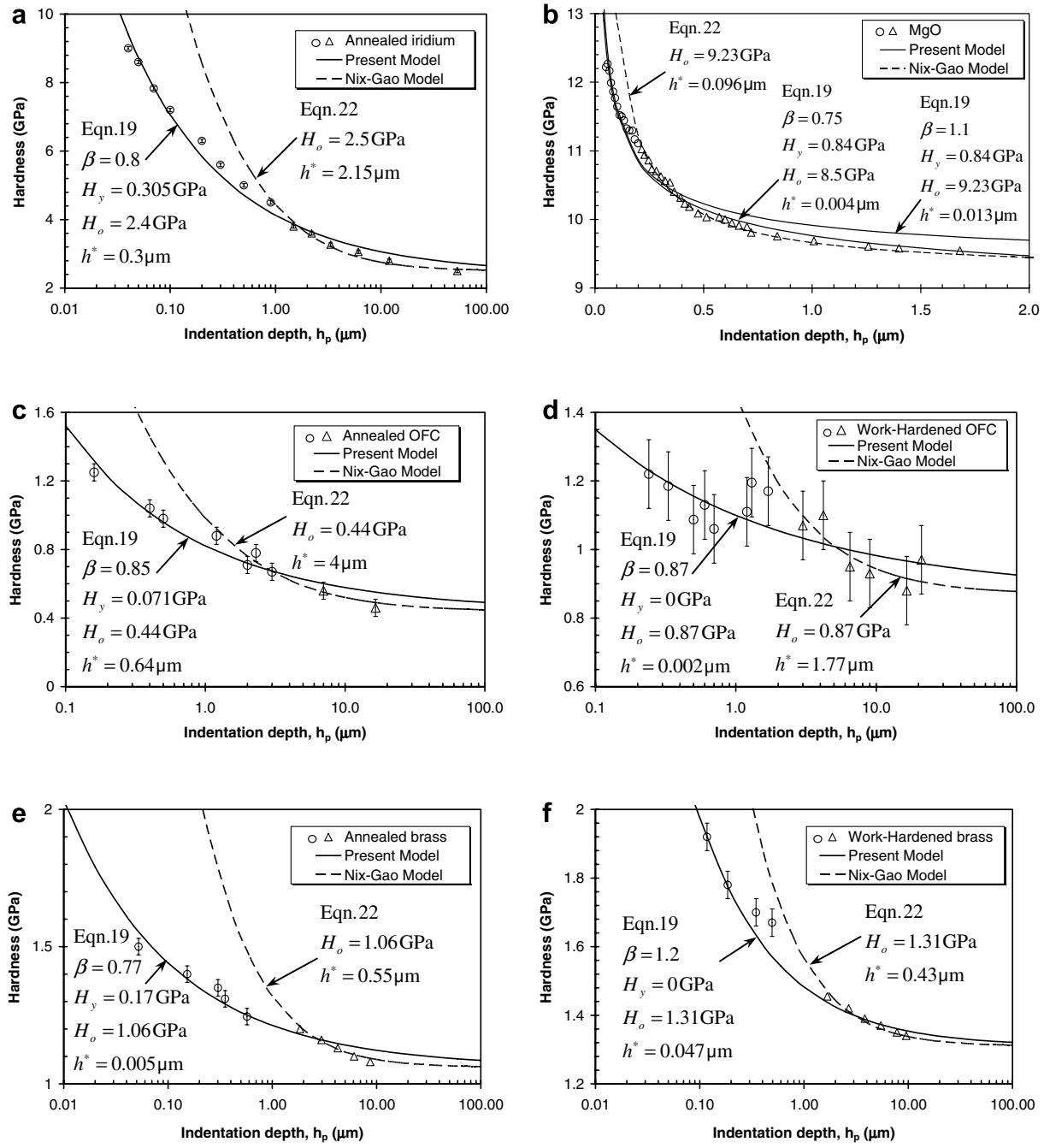

Fig. 4. Comparison of fit of the proposed model and Nix–Gao model to the experimental data: (a) annealed iridium (Swadener et al., 2002); (b) MgO (Feng and Nix, 2004); (c) annealed OFC (Lim and Chaudhri, 1999); (d) work-hardened OFC (Lim and Chaudhri, 1999); (e) annealed alpha-brass (Elmustafa and Stone, 2002) and (f) work-hardened OFC (Elmustafa and Stone, 2002). Δ and O designate microhardness and nanohardness data, respectively.

H_0 is slightly adjusted in order to get the best fit for both the micro and nanoindentation hardness data. Furthermore, it can be noticed from Fig. 4 that, generally, the present model slightly overpredicts the hardness at very large indentation depths, especially for MgO in Fig. 4b, because the ISE from the present model does not progressively vanish as fast as the experimental data. This is due to the fact that

Table 1
The parameters of the present ISE model, Eq. (19), and the calculation of the length scale parameter ℓ, Eq. (20), from the fitted hardness data

Material	β	H_y (GPa)	H_0 (GPa)	h^* (μm)	$\ell = h^*/\zeta$ (μm)	ISE index
Iridium (annealed)	0.8	0.305	2.4 (2.5)[a]	0.3 (2.15)	2.136	1.96
MgO	0.75	0.84	8.5 (9.23)	0.004 (0.096)	0.025	0.26
OFC (annealed)	0.85	0.071	0.44 (0.44)	0.64 (4.0)	4.53	2.71
OFC (cold-worked)	0.87	0	0.87 (0.87)	0.002 (1.77)	0.013	0.55
Alpha-brass (annealed)	0.77	0.17	1.06 (1.06)	0.005 (0.55)	0.036	0.36
Alpha-brass (cold-worked)	1.2	0	1.31 (1.31)	0.047 (0.43)	0.335	0.51

[a] The values between brackets are from the Nix–Gao model.

hardness data at larger indentation depths ($h > 10$ μm) should also be measured in order to accurately identify the macrohardness value H_0. Therefore, the noticed deviation of the present model at large indentation depths can be largely corrected by using smaller values for H_0 without affecting the predictions at shallow indentation depths. This is clearly demonstrated for MgO in Fig. 4b, where $H_0 = 8.5$ GPa gives better fit of the microhardness data than $H_0 = 9.23$ GPa. Moreover, despite the fact that results for indentation depths less than 100 nm are affected by tip rounding, the proposed model fits well both micro and nanohardness data although this effect is not considered in formulating the present model. However, it is shown in Huang et al. (2006) that the indenter tip radius effect alone cannot explain the nanoindentation size effect such that the ISE models of Qiu et al. (2001), Xue et al. (2002), and Qu et al. (2004), which incorporate this effect, provide only marginal improvements.

It can be noted from Table 1 that a zero value for the initial yield hardness H_y is used to fit the hardness data of both work-hardened OFC and Brass. This is attributed to the higher presence of prior dislocation density in the work-hardened specimen which triggers yielding immediately upon indenting the material surface whereas the corresponding annealed specimen yields after some amount of indentation. Therefore, the presence of prior dislocations affects the estimation of the material length parameter [see Eq. $(6)_1$] to yield higher hardness values. Furthermore, the work-hardened specimen has a reasonably perfect plastic behavior with a constant flow stress [see Lim and Chaudhri (1999) for stress-strain diagrams] such that the initial yield stress σ_y coincides with σ_0 in the power-law flow stress, Eq. $(3)_1$, where σ_0 scales with the macroscopic hardness H_0, Eq. (21).

It is believed that for $h < 0.1$ μm the dislocation density based models are limited and discrete dislocation models should be used instead. Therefore, the proposed model is limited for $h \geqslant 0.1$ μm although it gives good predictions for annealed iridium for $h < 0.1$ μm [see Fig. 4a]. The hardness $H_{0.1}$, which is the extrapolated hardness value at $h = 0.1$ μm, is used here as a representative value of the ISE. The last column in Table 1 presents the ISE index which is defined here as $(H_{0.1} - H_0)/H_0$. This index represents the increase in hardness as compared to the hardness at very large indentation depths (i.e. macrohardness). A larger value of the ISE index indicates a higher ISE and, therefore, it can be used to compare the ISE in different materials. Accordingly, it is noticed that the annealed OFC has the largest ISE and the largest material length scale $\ell = 4.53$ μm followed by annealed iridium with $\ell = 2.136$ μm. Thus, it can be generally concluded by comparing the values of the ISE index and the material length scales ℓ in Table 1 that the ISE increases as ℓ increases.

Moreover, it can be generally concluded that the ISE is most pronounced in annealed metallic materials whereas the effect is greatly reduced after cold working. This can be correlated to the change in the intrinsic material length scale due to the prior (initial) dislocation density as can be speculated from the physical nature of the length scale being in the order of spacing between dislocations, Eq. (6). One may, therefore, question the difference between the estimated values of ℓ for both annealed and work-hardened OFC and alpha-brass although they are obtained at the same plastic strain value of 7%. However, one can notice that ℓ for the work-hardened OFC is smaller than that for the annealed OFC. This indicates that the spacing between dislocations is reduced in the heavily work-hardened specimen due to the higher presence of prior dislocation density caused by the method of specimen preparation. In fact, Lim and Chaudhri (1999) reported that they have cold-worked OFC to a large strain value of approximately 60%. This means that

the work-hardened specimen initially contains higher dislocation density, or equivalently smaller spacing between dislocations, and thus smaller material length parameter. The presence of prior dislocations, thus, affects the estimation of the material length parameter to yield higher hardness values but lower ISE. Therefore, the shear stresses required to move dislocations in the work-hardened OFC will be higher than that required for the annealed OFC (owing to the interactions of nucleated dislocations with prior dislocations caused by work-hardening especially at shallow indentation depths). The hardness of the annealed OFC is thus smaller than that of the cold-worked OFC which is confirmed by the experimental results in Fig. 4c and d. In fact, it is shown through uniaxial compression tests of annealed and work-hardened OFC by Lim and Chaudhri (1999) that the work-hardening results in an increase in the flow stress of 0.29 GPa for work-hardened OFC compared to the flow stress of the annealed OFC at 1% plastic strain, which confirms the previous conclusion. Moreover, this indicates that materials with smaller ℓ are harder, and require greater loads to create the same contact area. Moreover, it can be concluded that the additional amount of hardening during deformation (i.e. ISE) increases as ℓ increases.

On the other hand, it can be noticed from Table 1 that the ISE in cold-worked brass and the corresponding length scale is larger than that of annealed brass, which is opposite to that for cold-worked and annealed OFC. However, the interaction coefficient β for annealed brass ($\beta = 0.77$) is less than that for cold-worked brass ($\beta = 1.2$), which implies, as is shown later in Section 5, that the total dislocation density in annealed brass is larger than that in cold-worked brass when the hardness is measured, although the initial dislocation density is higher in cold-worked brass. This is attributed to the work-hardening technique followed by Elmustafa and Stone (2002) that generated low initial dislocation density. This implies that ℓ, which is proportional to spacing between dislocations, of annealed brass should be smaller than that for cold-worked brass, which is the case in Table 1. This explains why the ISE in work-hardened brass is larger than in annealed brass. Therefore, this emphasizes again that as the length scale decreases as the ISE decreases.

It is noteworthy that the present model, Eq. (19), can equally well fit the experimental data even when neglecting the effects of the friction hardness, H_y, and the storage volume of the GNDs characterized by f. However, both H_y and f affect the magnitude of the material length scale significantly, Eq. (20), whereas the interaction coefficient β is not affected by H_y and f. Moreover, it can be seen from the values of h^* in Fig. 4a–f that when using Eq. (19) for fitting the micro and nanoindentation hardness data, smaller values for the material length scale parameter are identified than that obtained by the Nix–Gao model. Therefore, it can be concluded that the Nix–Gao model overestimates the length scale parameter whereas the values from Eq. (32) are in the order of the spacing between dislocations, which is more physically sound as suggested by Eq. $(6)_1$.

5. Discussion

As it is shown in the previous section that when fitting the experimental data to the ISE model in Eq. (22), one of the key issues is the suitable choice for a value of β. As seen in Eq. (1), this parameter has a physical meaning as it reflects the degree of interaction between SSDs and GNDs. Thus, it can be concluded from the hardness predictions in Fig. 4a–f that the discrepancy in the Nix–Gao model predictions at small indentations (i.e. nanoindentation) can be largely corrected by incorporating a nonlinear coupling between the densities of SSDs and GNDs, which is assessed here by the interaction coefficient β. Therefore, a simple arithmetic sum of the densities of SSDs and GNDs is a gross assumption especially at small indentation depths. Therefore, if one substitutes Eq. (2) into Eq. (1), one can express the total dislocation density, ρ_T, by

$$\rho_T^{\beta/2} = \rho_S^{\beta/2} + \rho_G^{\beta/2} \tag{28}$$

Eq. (28) reflects the physical process of dislocation interaction. Thus, β should be a material parameter that depends on the material microstructure. For $\beta = 2$, one can write

$$\rho_T = \rho_S + \rho_G \tag{29}$$

which is the main assumption adopted in formulating the Nix–Gao model. For $\beta < 2$, ρ_T is larger than the arithmetic sum of SSDs and GNDs given by Eq. (29) whereas for $\beta > 2$, ρ_T is smaller than the sum. Therefore, β either increases ($\beta < 2$) the effect of both kinds of dislocations or decreases ($\beta > 2$) such effect. However, Ashby (1970) has pointed out that in general the presence of GNDs will accelerate the rate of SSDs storage and that an arithmetic sum of their densities, Eq. (29), gives a lower limit on ρ_T so

that a higher total dislocation density can be obtained. Moreover, Alkorta et al. (2006) recently concluded that for a better quantitative agreement between the observed and predicted ISE, ρ_T under the indenter is required to be much denser than the very idealized assumption in the Nix–Gao model. Therefore, it is argued here that in order to properly estimate ρ_T, β should be less than 2.

It can be seen from the values of β in Table 1 that $\beta \approx 1$ such that ρ_T in Eq. (28) can be expressed by

$$\sqrt{\rho_T} = \sqrt{\rho_S} + \sqrt{\rho_G} \tag{30}$$

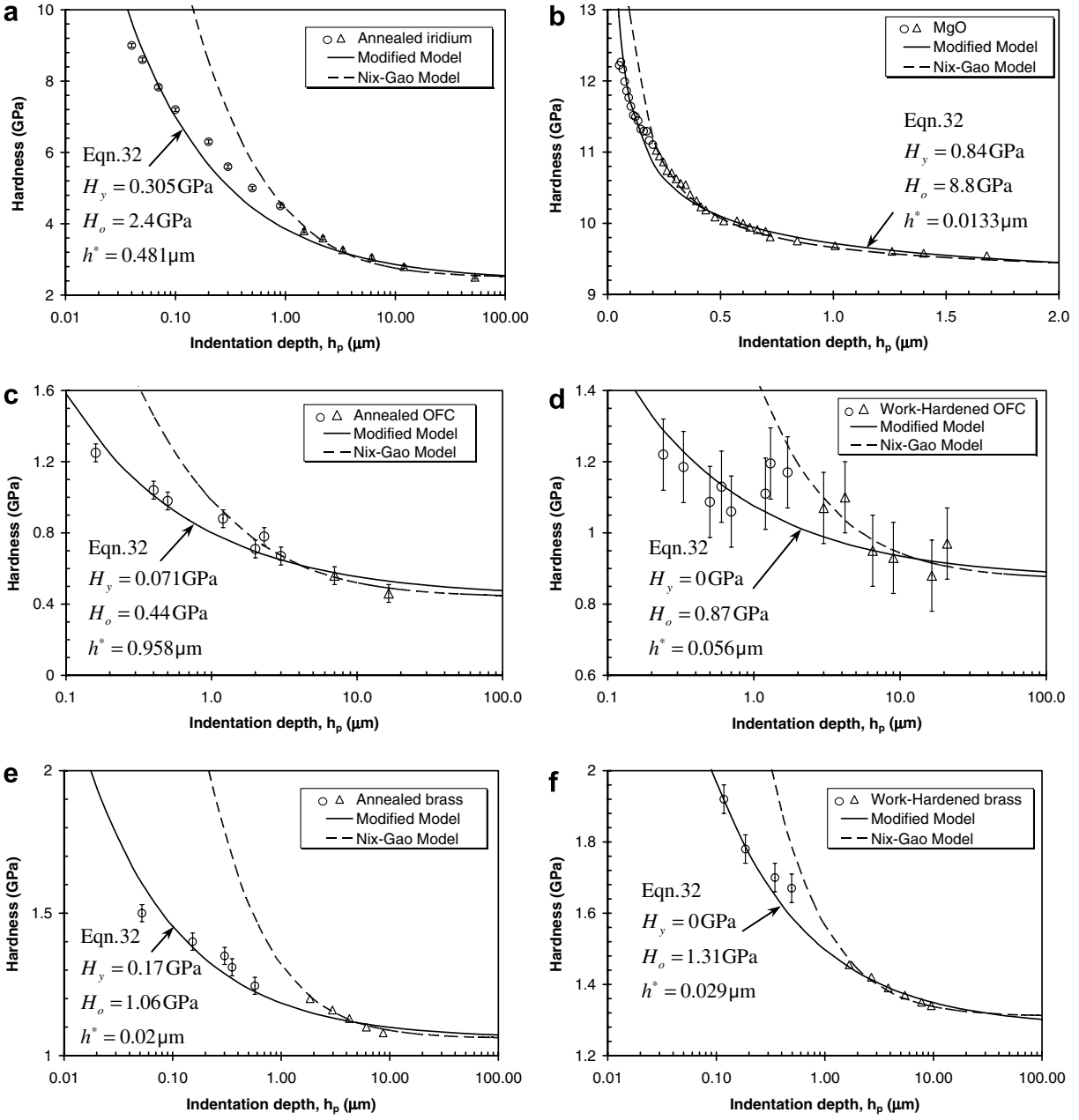

Fig. 5. Comparison of fit of the modified model and Nix–Gao model to the experimental data: (a) annealed iridium (Swadener et al., 2002); (b) MgO (Feng and Nix, 2004); (c) annealed OFC (Lim and Chaudhri, 1999); (d) work-hardened OFC (Lim and Chaudhri, 1999); (e) annealed alpha-brass (Elmustafa and Stone, 2002) and (f) work-hardened OFC (Elmustafa and Stone, 2002). Δ and O designate microhardness and nanohardness data, respectively.

which gives a total dislocation density larger than that given by Eq. (29). Therefore, one can conclude that the Nix–Gao model underestimates the total dislocation density such that it gives the lowest bound for the total dislocation density. Hence, for proper estimation of the total dislocation density, the flow stress in Eqs. (1) and (2) should be written as

$$\sigma = \sigma_y + \sigma_S + \sigma_G \tag{31}$$

Thus, it is argued here that a simple sum of the flow stress from SSDs and that from GNDs, Eq. (31), is more adequate than the simple sum of the densities of SSDs and GNDs, Eq. (29), when formulating the ISE model. Thus, setting $\beta = 1$ in Eq. (19) yields the following ISE model:

$$\left(\frac{H - H_y}{H_0 - H_y}\right) = 1 + \sqrt{\frac{h^*}{h_p}} \tag{32}$$

The degree to which the modified model in Eq. (32) can fit the experimental results is shown in Fig. 5a–f, where it is seen that this equations gives much better predictions of the micro and nanohardness values as compared to Nix–Gao model in Eq. (22). The values of the material parameters that correspond to the modified model in Eq. (32) are shown in Fig. 5a–f whereas the same parameters as in Fig. 4a–f are used for the Nix–Gao model predictions. Therefore, it can be concluded from the results in Fig. 5a–f that a simple sum of the flow stress due to SSDs to that due to GNDs, Eq. (31), gives better predictions of the ISE than the simple sum of the densities of SSDs and GNDs, Eq. (29), adapted in formulating the Nix–Gao model.

The values of the material length scale from the fitted hardness data in Fig. 5 are calculated in Table 2 from Eq. $(20)_1$ with $\zeta = 0.141$. Using the values listed in Table 2 for the magnitude of the Burgers vector b, the shear modulus G, the reference stress σ_0, the Nye's factor $\bar{r} = 2$, and the Taylor's factor $m = 3.08$ from the literature, one can estimate the coefficient α by using the estimated values for ℓ from its definition in Eq. (8) which yields reasonable values for α within the correct range (from 0.1 to 0.5). This proves the applicability of Eq. (8) and the proposed hardness model, Eq. (20), in identifying the material length scale parameter. However, it is noticed that the magnitude of ℓ from Eq. (8) is significantly affected by small variations in α.

Finally, it should be stated that the interaction coefficient β is considered until now as a phenomenological factor that lacks concrete dislocation mechanics-based interpretations. For establishing β as a real material parameter or interaction parameter more fundamental interpretations and discussions based on discrete dislocation dynamics simulations are necessary. Moreover, the proposed ISE model does not account for the indenter tip radius (Xue et al., 2002; Qu et al., 2004) and the indenter pile-up and sink-in (Begley and Hutchinson, 1998; Saha et al., 2001). These effects can be automatically accounted for by using the finite element method for the proposed strain gradient plasticity model in Eq. (3).

Table 2
Calculation of the length scale parameter ℓ from the fitted hardness data by the modified ISE model, Eq. (32), and by using Eq. (8)

Material	$\ell = h^*/\zeta$ (μm)	G (GPa)	σ_0 (GPa)	b (nm)	α Eq. (8)
Iridium (annealed)	3.411	217	2.85	0.271	0.34
MgO	0.095	126	4.54	0.298	0.15
OFC (annealed)	6.8	44	0.512	0.256	0.44
OFC (cold-worked)	0.4	44	0.36	0.256	0.1
Alpha-brass (annealed)	0.139	37	1.6	0.26	0.23
Alpha-brass (cold-worked)	0.205	37	0.5	0.26	0.1

6. Conclusions

A micromechanical model that assesses a nonlinear coupling between the statistically stored dislocations (SSDs) and the geometrically necessary dislocations (GNDs) is used in bridging the gap between the mesomechanical plasticity and the micromechanical plasticity. Based on this bridging an analytical expression is derived for the deformation-gradient-related intrinsic length scale parameter ℓ in terms of measurable microstructural physical parameters. This is done through the use of the strain gradient theory to bring closer together the microstructure (described by the Taylor's hardening law) and continuum (described by the strain hardening power-law) descriptions of plasticity. As a result ℓ is defined in terms of the average distance between dislocations, which characterizes the characteristic length of plasticity phenomenon.

The hardness predictions of the Nix and Gao (1998) ISE model deviate from the experimental results at small depths (i.e. nanoindentation) for conical or pyramidal indentations. A major correc-

tion of the Nix–Gao model that considers the correct dislocation density strengthening relationship has been proposed which succeeds in reproducing the deviation from the Nix–Gao relationship occurring at very low indentation depths. However, the correction of the plastic zone size in which GNDs are stored and the inclusion of the friction stress give marginal improvements to the predictions of the ISE model but significantly affect the identification of the material length scale parameter.

The most likely impediment in the Nix–Gao model is the assumption that the densities of SSDs and GNDs are coupled in a linear sense, such that $\rho_T = \rho_S + \rho_G$; i.e. the ideal assumption of all the obstacles being equally strong and equally spaced along a straight or curved contacting line. However, the real situation in experiments suggests that the hardening law cannot be taken as a simple sum of the densities of SSDs and GNDs. The total dislocation density under the indentation is larger than the simple sum of SSDs and GNDs such that it can be given by $\rho_T = [\rho_S^\gamma + \rho_G^\gamma]^{1/\gamma}$ where $\gamma < 1$. It is shown that the smaller the interaction coefficient γ, the more significant the interaction between SSDs and GNDs. Furthermore, it is shown through the set of predicted ISE data that $\gamma \approx 0.5$ gives a proper estimation of the total dislocation density. *This indicates that when using the Taylor's hardening law a simple sum of flow stresses from SSDs and GNDs is more adequate than the simple sum of SSD and GND densities*.

It is concluded that materials with smaller ℓ are harder and require greater loads in order to create the same contact area, which dictates that the additional amount of hardening during deformation increases as ℓ increases. Thus, the hardest materials have the smallest values of ℓ. It is also concluded that the size effect is more significant in annealed specimens than in cold-worked specimens. This implies that weaker materials exhibit higher ISE. Therefore, the ISE is expected to be influenced by both prior dislocations and the additional work hardening that occurs during indentation.

References

Abu Al-Rub, R.K., Voyiadjis, G.Z., 2004a. Analytical and experimental determination of the material intrinsic length scale of strain gradient plasticity theory from micro- and nano-indentation experiments. Int. J. Plast. 20, 1139–1182.

Abu Al-Rub, R.K., Voyiadjis, G.Z., 2004b. Determination of the material intrinsic length scale of gradient plasticity theory. Int. J. Multiscale Comput. Eng. 3 (3), 50–74.

Abu Al-Rub, R.K., Voyiadjis, G.Z., 2006. A physically based gradient plasticity theory. Int. J. Plast. 22, 654–684.

Alkorta, J., Martinez-Esnaola, J.M., Gil Sevillano, J., 2006. Detailed assessment of indentation size-effect in recrystallized and highly deformed niobium. Acta Mater. 54, 3445–3452.

Arsenlis, A., Parks, D.M., 1999. Crystallographic aspects of geometrically-necessary and statistically-stored dislocation density. Acta Mater. 47, 1597–1611.

Arsenlis, A., Parks, D.M., Becker, R., Bulatov, V.V., 2004. On the evolution of crystallographic dislocation density in non-homogeneously deforming crystals. J. Mech. Phys. Solids 52, 1213–1246.

Ashby, M.F., 1970. The deformation of plastically non-homogenous alloys. Philos. Maga. 21, 399–424.

Begley, M.R., Hutchinson, J.W., 1998. The mechanics of size-dependent indentation. J. Mech. Phys. Solids 46, 2049–2068.

Biwa, S., Storakers, B., 1995. An analysis of fully plastic Brinell indentation. J. Mech. Phys. Solids 43, 1303–1333.

Busso, E.P., Meissonnier, F.T., O'Dowd, N.P., 2000. Gradient-dependent deformation of two-phase single crystals. J. Mech. Phys. Solids 48, 2333–2361.

Chiu, Y.L., Ngan, A.H.W., 2002. A TEM investigation on indentation plastic zones in Ni3Al(Cr,B) single crystals. Acta Mater. 50, 2677–2691.

De Guzman, M.S., Neubauer, G., Flinn, P., Nix, W.D., 1993. The role of indentation depth on the measured hardness of materials. Mater. Res. Symp. Proc. 308, 613–618.

Durst, K., Backes, B., Franke, O., Goken, M., 2006. Indenation size effect in metallic materials: Modeling strength from pop-in to macroscopic hardness using geometrically necessary dislocations. Acta Mater. 54, 2547–2555.

Elmustafa, A.A., Stone, D.S., 2002. Indentation size effect in polycrystalline FCC metals. Acta Mater. 50, 3641–3650.

Feng, G., Nix, W.D., 2004. Indentation size effect in MgO. Scripta Mater 51, 599–603.

Fleck, N.A., Muller, G.M., Ashby, M.F., Hutchinson, J.W., 1994. Strain gradient plasticity: theory and experiment. Acta Metal. Mater. 42, 475–487.

Gao, H., Huang, Y., Nix, W.D., Hutchinson, J.W., 1999. Mechanism-based strain gradient plasticity – I. Theory. J. Mech. Phys. Solids 47, 1239–1263.

Gerberich, W.W., Tymiak, N.I., Grunlan, J.C., Horstemeyer, M.F., Baskes, M.I., 2002. Interpretation of indentation size effects. ASME Trans., J. Appl. Mech. 69, 433–442.

Haque, M.A., Saif, M.T.A., 2003. Strain gradient effect in nanoscale thin films. Acta Mater. 51, 3053–3061.

Hill, R., Storakers, B., Zdunek, A.B., 1989. A theoretical study of the Brinell hardness test. Proc. Roy. Soc. London Ser. A Math. Phys. Eng. Sci. 423 (1865), 301–330.

Huang, Y., Zhang, F., Hwang, K.C., Nix, W.D., Pharr, G.M., Feng, G., 2006. A model of size effects in nano-indentation. J. Mech. Phys. Solids 54, 1668–1686.

Huber, N., Nix, W.D., Gao, H., 2002. Identification of elastic–plastic material parameters from pyramidal indentation of thin films. Proc. Roy. Soc. London Ser. A 458 (2023), 1593–1620.

Johnson, K.L., 1970. The correlation of indentation experiments. J. Mech. Phys. Solids 18, 115–126.

Kiser, M.T., Zok, F.W., Wilkinson, D.S., 1996. Plastic flow and fracture of a particulate metal matrix composite. Acta Mater. 44, 3465–3476.

Kocks, U.F., 1966. A statistical theory of flow stress and work hardening. Phil. Mag. 13, 541.

Kramer, D., Huang, H., Kriese, M., Rohack, J., Nelson, J., Wright, A., Bahr, D., Gerberich, W.W., 1999. Yield strength predictions from the plastic zone around nanocontacts. Acta Mater. 47, 333–343.

Lim, Y.Y., Chaudhri, Y.Y., 1999. The effect of the indenter load on the nanohardness of ductile metals: an experimental study of polycrystalline work-hardened and annealed oxygen-free copper. Philos. Mag. A 79 (12), 2979–3000.

Lloyd, D.J., 1994. Particle reinforced aluminum and magnesium matrix composites. Int. Mater. Rev. 39, 1–23.

Ma, Q., Clarke, D.R., 1995. Size dependent hardness in silver single crystals. J. Mater. Res. 10, 853–863.

Mughrabi, H., 2001. On the role of strain gradients and long-range internal stresses in the composite model of crystal plasticity. Mater. Sci. Eng. A 317, 171–180.

Manika, I., Maniks, J., 2006. Size effects in micro- and nanoscale indentation. Acta Mater. 54, 2049–2056.

McElhaney, K.W., Valssak, J.J., Nix, W.D., 1998. Determination of indenter tip geometry and indentation contact area for depth sensing indentation experiments. J. Mater. Res. 13, 1300–1306.

Nan, C.-W., Clarke, D.R., 1996. The influence of particle size and particle fracture on the elastic/plastic deformation of metal matrix composites. Acta Mater. 44, 3801–3811.

Needleman, A., Gil Sevillano, J., 2003. Preface to the viewpoint set on: geometrically necessary dislocations and size dependent plasticity. Scripta Mater. 48 (2), 109–211.

Nix, W.D., Gao, H., 1998. Indentation size effects in crystalline materials: a law for strain gradient plasticity. J. Mech. Phys. Solids 46, 411–425.

Nye, J.F., 1953. Some geometrical relations in dislocated crystals. Acta Metal. 1, 153–162.

Oliver, W.C., Pharr, G.M., 1992. An improved technique for determining hardness and elastic modulus using load and displacement sensing indentation experiments. J. Mater. Res. 7, 1564–1583.

Orowan, E., 1948. Discussion in Symposium on Internal Stresses in Metals and Alloys. Institute of Metals, London, p. 451.

Poole, W.J., Ashby, M.F., Fleck, N.A., 1996. Micro-hardness of annealed and work-hardened copper polycrystals. Scripta Mater. 34, 559–564.

Qiu, X., Huang, Y., Nix, W.D., Hwang, K.C., Gao, H., 2001. Effect of intrinsic lattice resistance in strain gradient plasticity. Acta Mater. 49, 3949–3958.

Qu, S., Huang, Y., Nix, W.D., Jiang, H., Zhang, F., Hwang, K.C., 2004. Indenter tip radius effect on the Nix–Gao relation in micro- and nanoindentation hardness experiments. J. Mater. Res. 19, 3423–3434.

Saha, R., Xue, Z., Huang, Y., Nix, W.D., 2001. Indentation of a soft metal film on a hard substrate: strain gradient hardening effects. J. Mech. Phys. Solids 49, 1997–2014.

Shrotriya, P., Allameh, S.M., Lou, J., Buchheit, T., Soboyejo, W.O., 2003. On the measurement of the plasticity length scale parameter in LIGA nickel foils. Mech. Mater. 35, 233–243.

Stolken, J.S., Evans, A.G., 1998. A microbend test method for measuring the plasticity length-scale. Acta Mater. 46, 5109–5115.

Stelmashenko, N.A., Walls, M.G., Brown, L.M., Milman, Y.V., 1993. Microindentation on W and Mo oriented single crystals: an STM study. Acta Metal. Mater. 41, 2855–2865.

Swadener, J.G., George, E.P., Pharr, G.M., 2002. The correlation of the indentation size effect measured with indenters of various shapes. J. Mech. Phys. Solids 50, 681–694.

Tabor, D., 1951. The Hardness of Metals. Clarendon Press, Oxford.

Taylor, G.I., 1938. Plastic strain in metals. J. Inst. Metals 62, 307–324.

Voyiadjis, G.Z., Abu Al-Rub, R.K., 2005. Gradient plasticity theory with a variable length scale parameter. Int. J. Solids Struct. 42, 3998–4029.

Xue, Z., Huang, Y., Hwang, K.C., Li, M., 2002. The influence of indenter tip radius on the micro-indentation hardness. ASME J. Eng. Mater. Technol. 124, 371–379.

Yuan, H., Chen, J., 2001. Identification of the intrinsic material length in gradient plasticity theory from micro-indentation tests. Int. J. Solid. Struct. 38, 8171–8187.

Zhao, M., Slaughter, W.S., Li, M., Mao, S.X., 2003. Material-length-scale-controlled nanoindentation size effects due to strain-gradient plasticity. Acta Mater. 51, 4461–4469.